Journal of Power Sources 241 (2013) 578–582

Contents lists available at SciVerse ScienceDirect

Journal of Power Sources

journal homepage: www.elsevier.com/locate/jpowsour

Short communication

Tailoring the sealing properties of TiO_2–CaO–SrO–B_2O_3–SiO_2 glass-ceramic seals: Thermal properties, chemical compatibility and electrical property

Jialin Chen [a], Qi Zou [a], Fanrong Zeng [b], Shaorong Wang [b], Dian Tang [a], Hsiwen Yang [c], Teng Zhang [a,*]

[a] College of Materials Science and Engineering, Fuzhou University, Fuzhou, Fujian 350108, PR China
[b] CAS Key Laboratory of Materials for Energy Conversion, Shanghai Institute of Ceramics, Chinese Academy of Sciences (SICCAS), 1295 Dingxi Road, Shanghai 200050, PR China
[c] Department of Materials Science and Engineering, National United University, Miao-Li 36003, Taiwan, ROC

HIGHLIGHTS

- The addition of TiO_2 accelerates the crystallization of sealing glasses.
- Sealing properties of glasses changes with TiO_2 dopant due to structural change.
- Glass containing 4 mole % TiO_2 exhibits best sealing properties.

ARTICLE INFO

Article history:
Received 22 March 2013
Received in revised form
18 April 2013
Accepted 21 April 2013
Available online 9 May 2013

Keywords:
Solid oxide fuel cells
Glass-ceramic seals
Crystallization
Sealing properties

ABSTRACT

In this paper, TiO_2 is added to CaO–SrO–B_2O_3–SiO_2 sealing system to tailor the sealing properties of glass-ceramic seals. The coefficient of thermal expansion (CTE) of quenched glasses and glass-ceramics (held at 750 °C for 100 h) does not change significantly with the addition of TiO_2; whereas, the glass stability ($\Delta T_{xg} = T_x - T_g$) decreases systematically with increasing TiO_2. The addition of TiO_2 accelerates the crystallization of sealing glasses. The formation of Sr-containing phase, *e.g.*, $Sr(TiO_3)$, contributes to the improved chemical compatibility as well as the increase in conductivity of sealing glasses (*e.g.*, from 7.9×10^{-8} S cm^{-1} to 6.9×10^{-5} S cm^{-1} at 800 °C). In addition, the good bonding is observed at the interface between Cr-containing interconnect (430SS) and glasses containing 4–8 mole % TiO_2, held at 750 °C for 100 h.

1. Introduction

With the reduction of operational temperatures to under 800 °C, the design of Intermediate Temperature Solid Oxide Fuel Cells (IT-SOFCs) allows the use of ferritic stainless steels as interconnect components [1, 2]. However, the stability of IT-SOFCs under long-term operation or thermal cycles still remains challenging, due to mechanical stresses generated by the differences in thermal expansion of the involved materials as well as non-equilibrium thermal conditions upon heating and cooling. In particular, the interfacial reaction between glass-ceramic sealants and ferritic interconnects results in the formation of chromate phases, *e.g.*, $BaCrO_4$ and $SrCrO_4$, and consequently the physical separation of the sealants from interconnects [3–8].

Many efforts have been made on the modification of interconnects, including pre-oxidation [9–12], aluminizing [13,14] and protective coatings [15–18]. In addition, attention has also been focused on the chemical compatibility of sealing glasses [19–27]. However, the complex fixture of sealing couples restricts the precise analysis on the reaction and consequently results in the qualitative conclusions in most studies. Our recent work reported a quantitative analysis on the model reaction between sealing glass and Cr_2O_3 powders by UV–vis spectrum, which provides a reliable approach to evaluate the effect of different additives on the chemical compatibility of sealing glass [28,29]. It was also found that the controlled crystallization of sealing glass is beneficial or the chemical compatibility of sealing glass [30].

* Corresponding author. Tel.: +86 591 22866540; fax: +86 591 22866537.
E-mail address: Teng_zhang@fzu.edu.cn (T. Zhang).

0378-7753/$ – see front matter © 2013 Elsevier B.V. All rights reserved.
http://dx.doi.org/10.1016/j.jpowsour.2013.04.134

Table 1
Batch composition (in mole %) of sealing glasses.

Glass ID	SrO	CaO	B_2O_3	SiO_2	TiO_2
$2TiO_2$	25.48	25.48	3.92	43.12	2.00
$4TiO_2$	24.96	24.96	3.84	42.24	4.00
$6TiO_2$	24.44	24.44	3.76	41.36	6.00
$8TiO_2$	23.92	23.92	3.68	40.48	8.00

In this paper, TiO_2 was added systematically (from 2 to 8 mole %) into a representative CaO–SrO–B_2O_3–SiO_2 glass. Attention was focused on the compositional dependence of crystalline structure and sealing properties of sealing glasses with TiO_2 dopant to provide useful information for the design of reliable sealing system. The crystallized phases were determined by X-ray diffraction. The thermal properties of glasses, *e.g.,* glass transition temperature, softening temperature and coefficient of thermal expansion, were measured by differential scanning calorimetry and dilatometer. The chemical compatibility of sealing glasses was evaluated using the quantitative approach mentioned above [28,29]. The conductivity of glasses, in air from 600 to 800 °C, was measured using an impedance analyzer. The bonding interface between glasses and interconnects was analyzed by scanning electron microscopy and energy dispersive analysis.

2. Experimental

A 50 g sample of each glass was prepared by melting a homogeneous mixture of reagent grade alkaline earth carbonates, boric acid, and various oxides in a platinum crucible in air at 1400–1450 °C for 1 h. The nominal compositions of glasses (mole %) are shown in Table 1. Some of the melt was poured into stainless steel mold to obtain cylindrical shaped glass specimens (25 mm length and 6 mm diameter) and the rest of the melt was quenched on a steel plate to form the glass. Glass powders were then crushed and sieved to a particle size of 45–53 μm.

The glass transition temperature (T_g) and onset crystallization temperature (T_x) of glass powders were determined using differential scanning calorimetry (SDTQ600, TA, Inc.) at a heating rate of 10 °C min^{-1}. The dilatometric characteristics of quenched glasses, including the coefficient of thermal expansion (CTE, between 200 and 600 °C) and dilatometric softening temperature (T_d), were determined by dilatometer (DIL402C, NETZSCH, Inc.) at 5 °C min^{-1} in air. Some glass powders were held at 750 °C for 2 h (referred to as 'as-sealed species') and 100 h (referred to as 'long-term species'), respectively. Long-term species were also subjected to dilatometric measurements for comparison. Thermal properties of glasses and long-term species, including T_x, T_g, T_d and CTE, are summarized in Table 2. In addition, the crystalline phases in as-sealed and long-term species powders were identified by X-ray diffraction (XDS 2000, Scintag, Inc.). The crystalline content (weight %) in each as-sealed species was then calculated by RIQAS software (Release 4.0.0.8, Materials Data, Inc., CA).

A ~20 mg mixture of glass and 10 weight % Cr_2O_3 powders was reacted in an alumina boat in air at 750 °C for different time. The reaction product was dissolved into ~100 ml of deionized water and the absorption spectra were recorded using the UV–vis Spectrometer (Optima 2000 DV, Perkin Elmer, Inc.). The fraction of Cr^{6+} was then calculated by fitting the measured absorption to the calibration curve. The detailed procedure of this analysis has also been discussed elsewhere [28].

Some pellets (10 mm diameter and 2 mm thickness) were obtained by uniaxial pressing of glass powders and a subsequent crystallization at 750 °C for 100 h. The conductivity of long-term species, in air from 600 to 800 °C, was measured using an impedance analyzer (CHI660D, ChenHua, Inc.) in a frequency range from 0.1 Hz to 0.1 MHz, as described elsewhere [31].

The glasses were bonded to 430SS substrates and the interfacial reactions were characterized. Glass pastes were prepared by mixing ~50 mg glass powder (45–53 μm) with ~50 μl acetone. The pastes were applied to the ultrasonically-cleaned surfaces of 430SS. The coated samples were subsequently crystallized into long-term species in air at 750 °C for 100 h. The glass/metal sealing couples were cross-sectioned by a diamond saw and polished using SiC paper from 320 to 1200 grit, and then finished using an alumina suspension (3 μm). The polished samples were analyzed using field emission scanning electron microscopy (S4800, Hitachi, Inc.) and energy dispersive analysis by X-rays (EDAX, Hitachi, Inc.).

3. Results and discussion

Thermal properties of sealing glasses with TiO_2 dopant are summarized in Table 2. The glass transition temperature (T_g) of sealing glasses increases from 663 ± 3 to 678 ± 3 °C when the TiO_2 content increases from 2 to 8 mole %. In addition, the softening temperature (T_d) of sealing glasses with TiO_2 dopant increases from 718 ± 3 to 731 ± 3 °C when the TiO_2 content increases from 2 to 8 mole %, falling in the desired range of sealing temperature [32,33]. The onset crystallization temperature (T_x) of sealing glasses decreases from 793 °C for glass#2TiO_2 to 781 °C for glass#8TiO_2, consistent with the reduced crystallization temperatures in the TiO_2–AO–Al_2O_3–B_2O_3–SiO_2 (A = Ba, Ca and Mg) glasses [34]. The coefficient of thermal expansion (CTE, from 200 to 600 °C) of all glasses varies from (11.1 ± 0.1) × 10^{-6} to (11.3 ± 0.1) × 10^{-6} K^{-1}; whereas, the CTE of long-term species ranges from (9.6 ± 0.1) × 10^{-6} to (10.1 ± 0.1) × 10^{-6} K^{-1}.

Fig. 1a shows the XRD patterns of as-sealed species. Sr(TiO_3) (JCPDS Card No. 86-0179) is the primary phase in all glasses except for glass#2TiO_2, which still remains in amorphous state. In addition, the crystalline content increases from 0 weight % for glass#2TiO_2 to 45±5 weight % for glass#8TiO_2, in good agreement with the decrease in glass stability ($\Delta T_{xg} = T_x - T_g$) [35], from 130 °C for glass#2TiO_2 to 103 °C for glass#8TiO_2 (in Table 1). The degraded glass stability with TiO_2 dopant in the present work can be correlated with the reduced network connectivity of glasses [36,37]. The

Table 2
Thermal properties of sealing glasses.

Glass ID	T_g (°C)	T_x (°C)	T_d (°C)	$\Delta T_{xg} = T_x - T_g$ (°C)	CTE (×10^{-6} K^{-1}) glass (200–600 °C)	CTE (×10^{-6} K^{-1}) long-term species (200–600 °C)	Crystalline content (weight %), 750 °C for 2 h
$2TiO_2$	663 ± 3	793 ± 3	718 ± 3	130	11.3 ± 0.1	10.1 ± 0.1	0
$4TiO_2$	668 ± 3	787 ± 3	721 ± 3	119	11.2 ± 0.1	9.9 ± 0.1	19 ± 5
$6TiO_2$	671 ± 3	783 ± 3	726 ± 3	112	11.2 ± 0.1	9.6 ± 0.1	38 ± 5
$8TiO_2$	678 ± 3	781 ± 3	731 ± 3	103	11.1 ± 0.1	9.8 ± 0.1	45 ± 5

T_g: glass transition temperature.
T_x: onset crystallization temperature.
T_d: dilatometric softening temperature.
ΔT_{xg}: glass forming ability.
CTE: coefficient of thermal expansion.

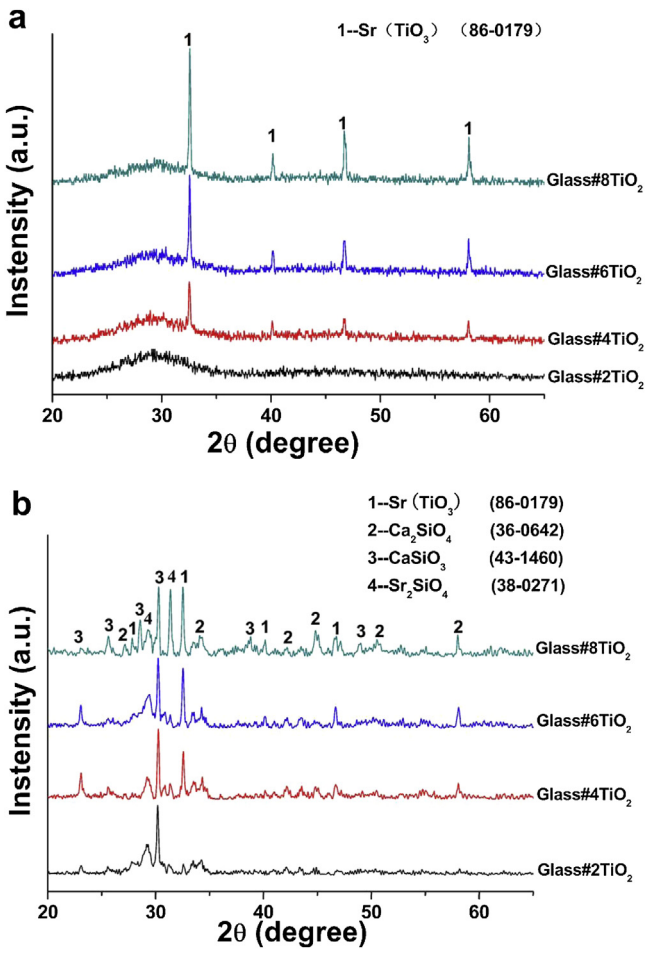

Fig. 1. XRD patterns of glass-ceramics, (a) as-sealed species and (b) long-term species.

XRD patterns of long-term species are also included for comparison (in Fig. 1b). The main phases in long-term species include Sr_2SiO_4 (JCPDS Card No. 38-0271), Ca_2SiO_4 (JCPDS Card No. 36-0642), $CaSiO_3$ (JCPDS Card No. 43-1460) and $Sr(TiO_3)$. It is interesting to note that the intensity of diffraction peaks corresponding for $Sr(TiO_3)$ increases with increasing TiO_2 content, which indicates that greater amounts of $Sr(TiO_3)$ form in glasses with more TiO_2 dopant.

Shown in Fig. 2 are the absorption of Cr^{6+} (left *Y*-axis) and the fraction of Cr^{6+} (right Y-axis) in the reaction couples between Cr_2O_3 and glass powders, after reacting in air at 750 °C for different time. The fraction of Cr^{6+} in all samples increases with increasing reaction time. For example, the fraction of Cr^{6+} in the reaction couples between Cr_2O_3 and glass#4TiO_2 increases from 38 to 47% when the reaction time increases from 1 to 7 h. In addition, the fraction of Cr^{6+} in the reaction couples decreases with increasing TiO_2 dopant. For example, the fraction of Cr^{6+}, after reacting in air at 750 °C for 7 h, decreases from 50% for glass#2TiO_2 to 35% for glass#8TiO_2.

Fig. 3 shows the temperature dependence of conductivity (log σ versus 1000 T^{-1}) for pellets of long-term species measured in air from 600 to 800 °C. The conductivity (σ) of all species increases with increasing temperature. In addition, the conductivity of all species at each temperature increases with TiO_2 dopant. For example, the conductivity (σ) of all species at 800 °C increases from 1.6×10^{-7} S cm^{-1} for glass#2TiO_2 to 6.9×10^{-5} S cm^{-1} for glass#8TiO_2, meeting the insulating requirement of sealing glasses ($<10^{-4}$ S cm^{-1}) [38,39]. The increase in conductivity of glass-ceramics with TiO_2 dopant in the present work can be attributed

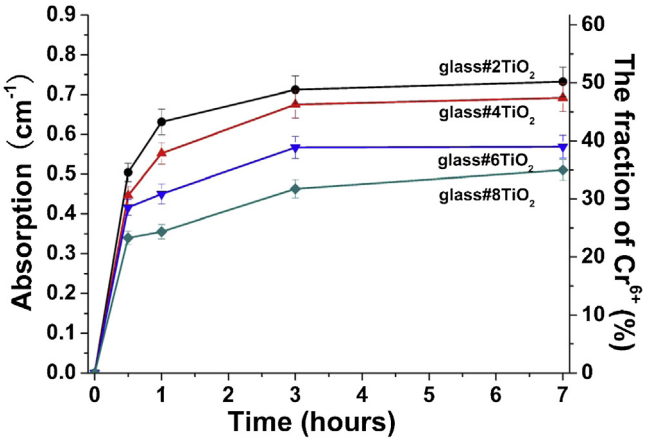

Fig. 2. The absorption of Cr^{6+} (left *Y*-axis) and the fraction of Cr^{6+} (right *Y*-axis) in the reaction couples between Cr_2O_3 and glass powders, after reacting in air at 750 °C for different time.

to not only the formation of $Sr(TiO_3)$ ($\sim 7.0 \times 10^{-4}$ S cm^{-1} [40]) but the improved movement of charge carriers in residual glasses due to the reduced network connectivity with network modifier.

Shown in Fig. 4 are micrographs of the interfaces between long-term species and 430SS. These images were taken near the edges of each sample. Also shown are EDS elemental line scans taken across the respective interfaces. The physical separation of glass from the interconnect can be observed in the sealing couple of glass#2TiO_2/430SS (in Fig. 4a), due to the extensive formation of $SrCrO_4$ (in Fig. 2); whereas, a continuous interface forms in other sealing couples of glass/430SS (in Fig. 4b–d). The diffusion of elements, *e.g.*, Cr and Sr, occurs between glasses and interconnects, depending on the extent of interfacial reaction. In addition, the number of whitish grain boundaries in glass side increases with increasing TiO_2 content, consistent with greater intensity of diffraction peaks corresponding for $Sr(TiO_3)$ with more TiO_2 dopant (in Fig. 1b).

The crystallization characteristics, *e.g.*, crystallization sequence and crystalline content, play an important role in determining the properties of glass-ceramic sealants, including sealing properties [33,41] as well as high-temperature mechanical properties [42]. Therefore, numerous nucleation agents have been investigated to change the crystallization process and consequently the properties of glasses [43,44]. It has also been found that Sr^{2+} ions in crystalline (such as Sr_2SiO_4 and $Sr(TiO_3)$) are thermodynamically more stable than those in a glass matrix [30]. The addition of TiO_2 in the present

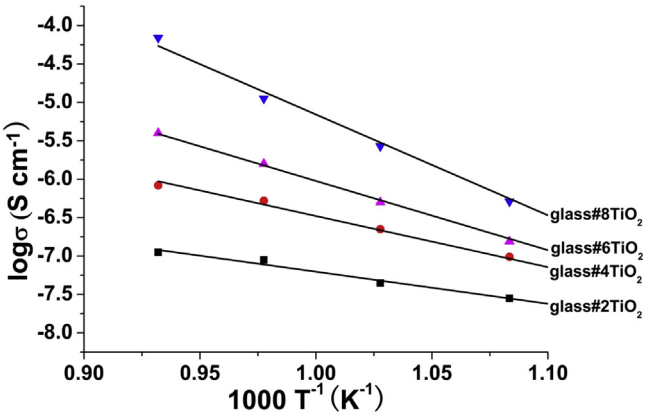

Fig. 3. The temperature dependence of conductivity (log σ versus 1000 T^{-1}) for pellets of long-term species measured in air from 600 to 800 °C.

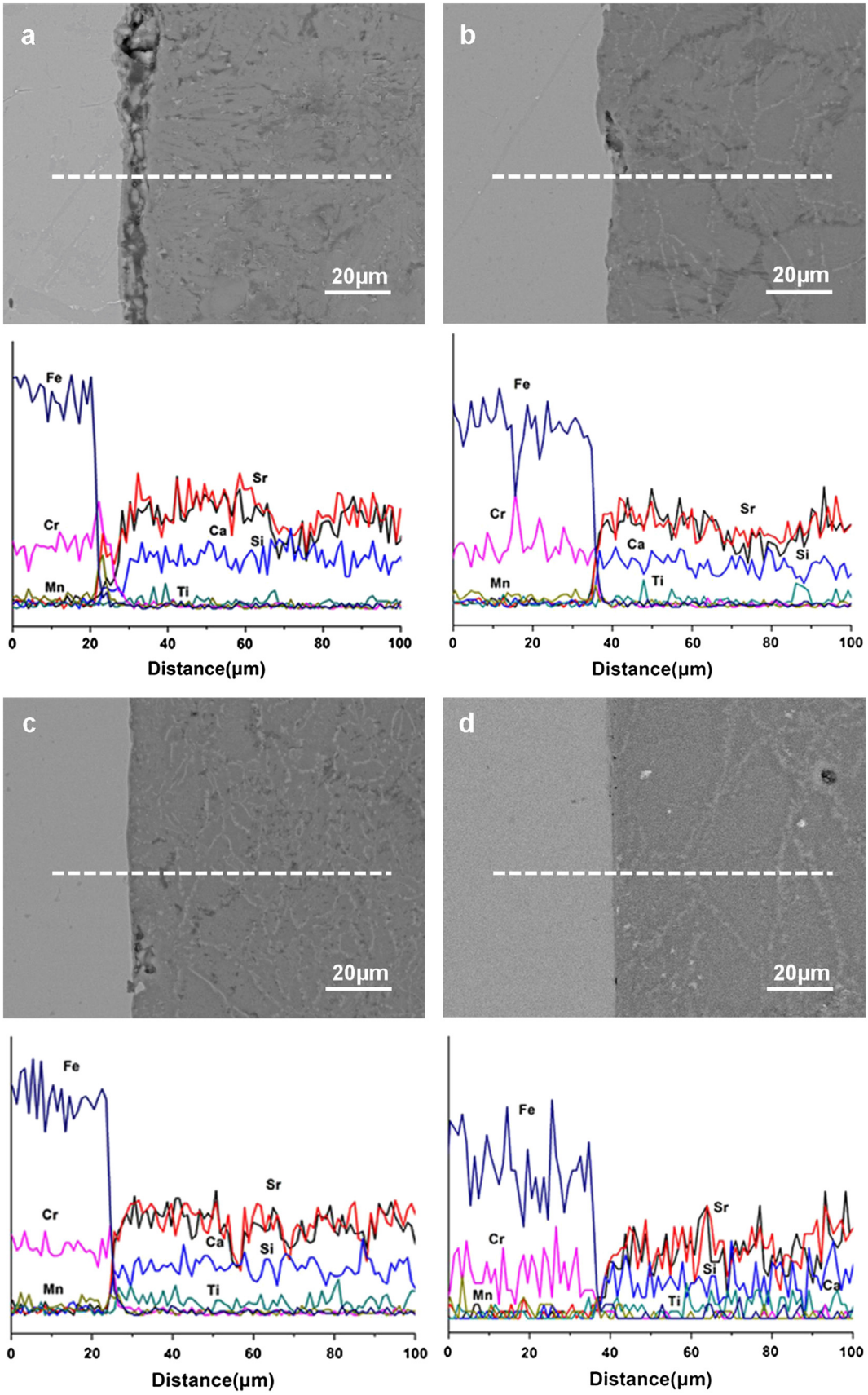

Fig. 4. Micrographs of the interfaces between long-term species and 430SS and EDS elemental line scans taken across the respective interfaces, (a) glass#2TiO_2, (b) glass#4TiO_2, (c) glass#6TiO_2 and (d) glass#8TiO_2.

work accelerates the crystallization of Sr-containing phases, *e.g.*, $Sr(TiO_3)$ and Sr_2SiO_4 (in Fig. 1), which contributes to the improved chemical compatibility (in Fig. 2) as well as good bonding between glasses containing 4–8 mole % TiO_2 and 430SS (in Fig. 4b–d). In addition, the formation of $Sr(TiO_3)$ and the reduced network connectivity of glasses with TiO_2 dopant contribute to the increase in the conductivity of long-term species (in Fig. 3). Therefore, the glass containing 4 mole% TiO_2 exhibits best sealing properties, considering sealing temperature window, chemical compatibility and electrical conductivity.

4. Conclusions

The effect of TiO_2 on the crystalline structures and sealing properties of $CaO–SrO–B_2O_3–SiO_2$ sealing glasses is systematically investigated in the present work. The addition of TiO_2 accelerates the formation of Sr-containing phases, $Sr(TiO_3)$ and Sr_2SiO_4. Sealing properties of glasses, including thermal properties, chemical compatibility and electrical property, also change by the addition of TiO_2. The glass containing 4 mole % TiO_2 exhibits best sealing properties. The founding on the compositional dependence of crystalline structures and sealing properties of $CaO–SrO–B_2O_3–SiO_2–TiO_2$ glasses will shed lights onto the design of sealing glasses for IT-SOFCs.

Acknowledgments

The authors gratefully acknowledge the financial support of the National Natural Science Foundation of China (No. 51102045), the Ph.D. Programs Foundation of Ministry of Education of China (No. 20103514120006), program for New Century Excellent Talents in Fujian Province University (No. JA12013), and funds for Distinguished Young Scientists from the Fujian Education Department (No. JA11007). They would also like to thank Dr. Brow (MS&T) for critical comments, Jianhang Lin for assistance with SEM/EDS, Qingming Huang for assistance with X-ray diffraction, Fen Lin for assistance with DSC analysis.

References

[1] Z. Yang, K.S. Weil, D.M. Paxton, J.W. Stevenson, Journal of The Electrochemical Society 150 (2003) A1188–A1201.
[2] P. Kofstad, R. Bredesen, Solid State Ionics 52 (1992) 69–75.
[3] Z. Yang, Solid State Ionics 160 (2003) 213–225.
[4] Z. Yang, G. Xia, K.D. Meinhardt, S.K. Weil, J.W. Stevenson, Journal of Materials Engineering and Performance 13 (2004) 327–334.
[5] Y.-S. Chou, J.W. Stevenson, R.N. Gow, Journal of Power Sources 170 (2007) 395–400.
[6] K.D. Meinhardt, D.S. Kim, Y.S. Chou, K.S. Weil, Journal of Power Sources 182 (2008) 188–196.
[7] M.K. Mahapatra, K. Lu, Journal of Materials Science 44 (2009) 5569–5578.
[8] L. Peng, Q. Zhu, Journal of Power Sources 194 (2009) 880–885.
[9] F. Smeacetto, M. Salvo, M. Ferraris, J. Cho, A.R. Boccaccini, Journal of The European Ceramic Society 28 (2008) 61–68.
[10] B. Kuhn, E. Wessel, J. Malzbender, R.W. Steinbrech, L. Singheiser, International Journal of Hydrogen Energy 35 (2010) 9158–9165.
[11] C.-K. Lin, J.-Y. Chen, J.-W. Tian, L.-K. Chiang, S.-H. Wu, Journal of Power Sources 205 (2012) 307–317.
[12] Y.-S. Chou, J.W. Stevenson, P. Singh, Journal of Power Sources 184 (2008) 238–244.
[13] Y.S. Chou, J.W. Stevenson, P. Singh, Journal of Power Sources 185 (2008) 1001–1008.
[14] J.P. Choi, K. Scott Weil, Y. Matt Chou, J.W. Stevenson, Z. Gary Yang, International Journal of Hydrogen Energy 36 (2011) 4549–4556.
[15] V. Kumar, S. Sharma, O.P. Pandey, K. Singh, Solid State Ionics 181 (2010) 79–85.
[16] M.K. Mahapatra, K. Lu, International Journal of Hydrogen Energy 35 (2010) 11908–11917.
[17] Y.-S. Chou, E.C. Thomsen, J.P. Choi, J.W. Stevenson, Journal of Power Sources 202 (2012) 149–156.
[18] Y.S. Chou, J.W. Stevenson, G.G. Xia, Z.G. Yang, Journal of Power Sources 195 (2010) 5666–5673.
[19] Y.-S. Chou, E.C. Thomsen, R.T. Williams, J.P. Choi, N.L. Canfield, J.F. Bonnett, J.W. Stevenson, A. Shyam, E. Lara-Curzio, Journal of Power Sources 196 (2011) 2709–2716.
[20] N. Laorodphan, P. Namwong, W. Thiemsorn, M. Jaimasith, A. Wannagon, T. Chairuangsri, Journal of Non-Crystalline Solids 355 (2009) 38–44.
[21] F. Smeacetto, A. Chrysanthou, M. Salvo, Z. Zhang, M. Ferraris, Journal of Power Sources 190 (2009) 402–407.
[22] S. Ghosh, A.D. Sharma, A.K. Mukhopadhyay, P. Kundu, R.N. Basu, International Journal of Hydrogen Energy 35 (2010) 272–283.
[23] A. Goel, D.U. Tulyaganov, V.V. Kharton, A.A. Yaremchenko, J.M.F. Ferreira, Journal of Power Sources 195 (2010) 522–526.
[24] M. Bram, L. Niewolak, N. Shah, D. Sebold, H.P. Buchkremer, Journal of Power Sources 196 (2011) 5889–5896.
[25] Chou Yeong-Shyung, E.C. Thomsen, J.P. Choi, J.W. Stevenson, Journal of Power Sources 197 (2012) 154–160.
[26] G. Kaur, O.P. Pandey, K. Singh, International Journal of Hydrogen Energy 37 (2012) 3883–3889.
[27] Y. Ye, D. Yan, X. Wang, J. Pu, B. Chi, L. Jian, International Journal of Hydrogen Energy 37 (2012) 1710–1716.
[28] T. Zhang, H. Zhang, G. Li, H. Yung, Journal of Power Sources 195 (2010) 6795–6797.
[29] T. Zhang, R.K. Brow, W.G. Fahrenholtz, S.T. Reis, Journal of Power Sources 205 (2012) 301–306.
[30] T. Zhang, Q. Zou, F. Zeng, S. Wang, D. Tang, H. Yang, Journal of Power Sources 216 (2012) 1–4.
[31] C. Lara, M.J. Pascual, R. Keding, A. Durán, Journal of Power Sources 157 (2006) 377–384.
[32] J.W. Fergus, Journal of Power Sources 147 (2005) 46–57.
[33] S.T. Reis, M.J. Pascual, R.K. Brow, C.S. Ray, T. Zhang, Journal of Non-Crystalline Solids 356 (2010) 3009–3012.
[34] N. Lahl, D. Bahadur, K. Singh, L. Singheiser, K. Hilpert, Journal of The Electrochemical Society 149 (2002) A607–A614.
[35] E.B. Ferreira, E.D. Zanotto, S. Feller, G. Lodden, J. Banerjee, T. Edwards, M. Affatigato, Journal of The American Ceramic Society 94 (2011) 3833–3841.
[36] A.W. Wren, F.R. Laffir, A. Kidari, M.R. Towler, Journal of Non-Crystalline Solids 357 (2011) 1021–1026.
[37] M.K. Mahapatra, K. Lu, Journal of Power Sources 185 (2008) 993–1000.
[38] M.K. Mahapatra, K. Lu, Materials Science and Engineering: R: Reports 67 (2010) 65–85.
[39] P.A. Lessing, Journal of Materials Science 42 (2007) 3465–3476.
[40] Q.X. Fu, S.B. Mi, E. Wessel, F. Tietz, Journal of The European Ceramic Society 28 (2008) 811–820.
[41] S.-F. Wang, Y.-F. Hsu, H.-C. Lu, S.-C. Lo, C.-S. Cheng, International Journal of Hydrogen Energy 37 (2012) 5901–5913.
[42] H.-T. Chang, C.-K. Lin, C.-K. Liu, Journal of Power Sources 195 (2010) 3159–3165.
[43] K. Sharma, G.P. Kothiyal, L. Montagne, F.O. Méar, B. Revel, International Journal of Hydrogen Energy 37 (2012) 11360–11369.
[44] T. Sun, H. Xiao, W. Guo, X. Hong, Ceramics International 36 (2010) 821–826.